Inorganic Chemistry

ARTICLE

pubs.acs.org/IC

Morphological Evolution of $(NH_4)_{0.5}V_2O_5 \cdot mH_2O$ Fibers into Belts, Triangles, and Rings

Gujjarahalli Thimmanna Chandrappa,*[,†] Pallellappa Chithaiah,[†] Siddaramanna Ashoka,[†] and Jacques Livage[‡]

[†]Department of Chemistry, Bangalore University, Bangalore 560001, India

[‡]Chimie de la Matière Condensée, Collège de France, 11 place Marcelin Berthelot, 75231 Paris, France

Supporting Information

ABSTRACT: In this contribution, single-crystalline $(NH_4)_{0.5}V_2O_5 \cdot mH_2O$ xerogels made of belts, rings, triangles, and ovals have been synthesized using a surfactant-free hydrothermal method. The analytical techniques of scanning electron microscopy (SEM), transmission electron microscopy (TEM), powder X-ray diffraction (PXRD), thermogravimetric analysis (TGA), energy dispersive X-ray spectroscopy (EDX), Fourier transform infrared (FTIR), high-resolution TEM (HRTEM), and selected area electron diffraction (SAED) have been used to characterize the morphology, composition, and structure of the as-prepared products. On the basis of SEM and TEM observations, we suggested that the as-prepared $(NH_4)_{0.5}V_2O_5 \cdot mH_2O$ rings, triangles, and ovals have been formed by connecting two ends of the vanadium oxide sheet made of edge and corner sharing VO_5 square pyramids. The as-prepared $(NH_4)_{0.5}V_2O_5 \cdot mH_2O$ nanobelts are up to several hundreds of micrometers long, 402−551 nm wide, and 235−305 nm thick. The thickness and width of the rings are respectively ∼454 nm and ∼1 μm. Triangles with three unequal sides having a thickness of ∼143 nm and a width of ∼1 μm were also formed. The crystalline orthorhombic phase of shcherbianite V_2O_5 was obtained on calcination of $(NH_4)_{0.5}V_2O_5 \cdot mH_2O$ at 350 °C for 2 h. The SEM image of this V_2O_5 product retains the parent morphology of the preheated compound. A possible reaction mechanism and the growth process involved in the formation of belts/rings/triangles and ovallike microstructures are discussed.

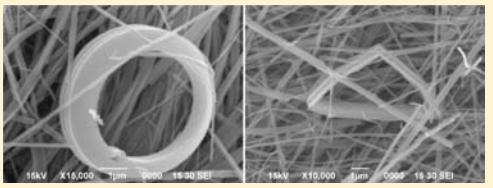

1. INTRODUCTION

Nanostructured transition metal oxides have been extensively studied during the past few years.[1] Among them, vanadium oxide based compounds received significant attention, due to their structural flexibility combined with chemical and physical properties. They find a wide range of potential applications in high energy density lithium ion batteries,[2] catalysis,[3] electrochromic devices,[4] actuators,[5] and sensors.[6]

Vanadium oxides exhibit a layered structure and are well-known for their intercalation properties. Among them, cation intercalated xerogels $M_xV_2O_5 \cdot mH_2O$ (M = Li^+, NH_4^+, and Na^+) have been extensively studied for their electrochemical properties.[7a] They are made of V_2O_5 bilayers whose interlayer space is occupied by water molecules ($V_2O_5 \cdot mH_2O$) and cations ($M_xV_2O_5 \cdot mH_2O$). $M_xV_2O_5 \cdot mH_2O$ xerogels show significant differences from $V_2O_5 \cdot mH_2O$ xerogels. Due to cations intercalated between VO_5 pyramid sheets, $M_xV_2O_5 \cdot mH_2O$ xerogels exhibit better electrochemical properties than $V_2O_5 \cdot mH_2O$ xerogels. In ($(NH_4)_{0.5}V_2O_5 \cdot mH_2O$), NH_4^+ that is intercalated between the vanadium oxide layers can be reversibly exchanged by various cations such as Li^+, Na^+, K^+, or Ca^{2+} to form new $M_xV_2O_5 \cdot mH_2O$ nanostructures.[7b] Moreover, intercalated NH_4^+ ions can be easily removed upon calcination without altering the original morphology.

A large variety of vanadium oxide based compounds have been described, in which cations, transition metal complexes, organic molecules, and even polymers have been intercalated. For instance, Nesper et al.[8] synthesized vanadium oxide nanotubes via the intercalation of primary alkylamines. Luca et al.[9,10] prepared mesoporous sieves of vanadium oxide via the intercalation of tetramethylammonium cations. In a previous publication,[11] we reported nanostructured vanadium pentoxide foams obtained through a new soft-chemical route by adding hexadecylamine to crystalline vanadium pentoxide followed by the addition of hydrogen peroxide at room temperature.

Various morphologies of vanadium oxide and derived compounds such as nanotubes, wires, fibers, belts, rods, and mesoporous structures in micro-/nanostructures have so far been successfully synthesized by using a variety of synthetic routes.[12−17] Recently, nanorings/springs/helical structures for a number of inorganic materials such as CuO,[18] SnO_2,[19] InGaN,[20] α-Ga_2O_3,[21] InP nanosprings,[22] PbSe,[23] BN,[24] AlN,[25] ZnO,[26−29] gold,[30] Zn_2SnO_4,[31] amorphous SiO_2,[32] SiC nanosprings,[33] and carbon nanotube coils[34] have been reported. To the best of our knowledge, $(NH_4)_{0.5}V_2O_5 \cdot mH_2O$ ring/triangle and oval forms have not been reported so far. Here, we report for the first time such unusual kinds of morphologies which may find potential use in future generations of microelectronics, sensing devices, nanoprobes, and even nanomedicine due to their size and special morphology-related properties.

Received: November 15, 2010
Published: July 20, 2011

2. EXPERIMENTAL SECTION

2.1. Sample Preparation. Chemical reagents of analytical grade were purchased from Merck Ltd. and utilized without further purification. Double distilled water was used throughout the experiments. The typical procedure we followed for the synthesis of vanadium oxide microstructures is as follows. Ammonium metavanadate (0.25 g) was dissolved in hydrogen peroxide solution (0.5 mL, 30%) to form a clear, yellow solution. A citric acid solution (30 mL, 0.01M) was then added, resulting in the formation of a red solution that was stirred for 15 min. The obtained clear red solution was transferred into a Teflon-lined stainless steel autoclave with a capacity of 50 mL and then sealed, and the autoclave was maintained at 160 °C for 48 h. After hydrothermal treatment, the autoclaves were naturally cooled to ambient temperature. The spongy-brown product was harvested by centrifugation, washed several times with distilled water and absolute alcohol to remove any possible residual impurities, and finally dried at 60 ° C in an oven for 2 h.

2.2. Sample Characterization. The crystallographic information of the samples was investigated by powder X-ray diffraction (PXRD). The XRD patterns with diffraction intensity versus 2θ were recorded on a Philips X'pert PRO X-ray diffractometer with a graphite monochromatized Cu Kα radiation source (λ = 1.541 Å) operated at 40 kV and 30 mA. The morphologies of the products were examined by Quanta-200 scanning electron microscope (SEM) equipped with an energy dispersive X-ray spectroscopy (EDX). Samples were gold-coated prior to SEM analysis. The nano-/microstructure of the products was observed by transmission electron microscopy (TEM) performed with a Hitachi model H-600 instrument operating at 100 kV. High-resolution transmission electron microscopy (HRTEM) images and selected area electron diffraction (SAED) patterns were taken with a JEOL 3011, 300 kV instrument with an ultrahigh-resolution (UHR) pole piece. Samples for TEM were prepared by dropping the dispersion on amorphous carbon films supported on a copper grid and drying the grids in air. The Fourier transform infrared (FTIR) spectra of the product dispersed in a KBr pellet were recorded on a FTIR Nicolet spectrometer over the range of 400−4000 cm^{-1}. Thermal gravimetric analysis (TGA) of the sample was carried out on a Shimadzu TA-50 thermal analyzer at a heating rate of 10 °C min^{-1} up to 600 °C in an air.

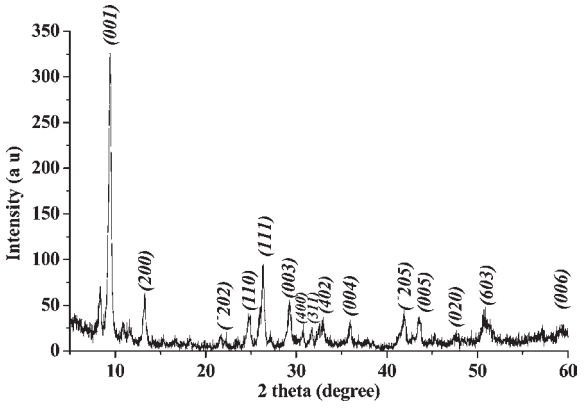

Figure 1. PXRD pattern of $(NH_4)_{0.5}V_2O_5 \cdot mH_2O$ product.

3. RESULTS AND DISCUSSION

The PXRD pattern of the sample prepared through hydrothermal method is shown in Figure 1. All of the diffraction peaks on the curve match the standard data of monoclinic $(NH_4)_{0.5}V_2O_5 \cdot mH_2O$ [JCPDS No. 31-0075; $(NH_4)\ V_4O_{10} \cdot mH_2O$ may be regarded as $(NH_4)_{0.5}V_2O_5 \cdot mH_2O$)]. The XRD pattern of the product exhibits the (00*l*) peak series in which the (002) harmonic is missing, suggesting that the double-layer structure of the $(NH_4)_{0.5}V_2O_5 \cdot mH_2O$ network is preserved. The X-ray pattern of the product also exhibits the *hkl* set of reflections, suggesting that the ordered stacking of the NH_4^+ intercalated V_2O_5 belts is not markedly present in the product.[14b] The basal distance estimated from the PXRD pattern for a strong (001) peak (~9.4 Å) is close to that observed for NH_4^+ intercalated xerogels.[35] The presence of salts or bases during the formation of the vanadium oxide gels favors the intercalation of the corresponding cations between the vanadium oxide layers. The smaller interplanar spacing of the obtained product (~9.4 Å) as compared to 11.5 Å in $V_2O_5 \cdot nH_2O$ xerogel should be due to the intercalation of ammonium ions that decreases the amount of water molecules. The presence of ammonium ions may introduce attractive electrostatic forces between the vanadium oxide layers, which is in good agreement with what has been reported in the literature.[35,36]

The FTIR spectrum of the as-prepared sample is shown in Figure 2A. The band centered at 981 cm^{-1} is assigned to V═O stretching vibration, which is sensitive to intercalation and suggests that NH_4^+ ions are inserted between the vanadium oxide layers, in full agreement with previous results.[36] The splitting of this 981 cm^{-1} band into two absorption peaks

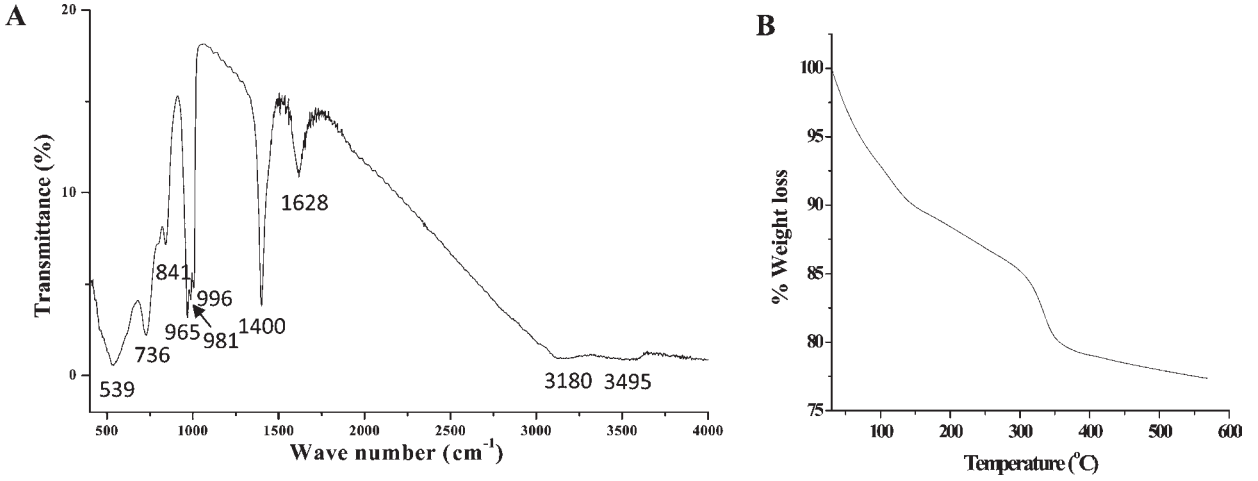

Figure 2. (A) FTIR spectrum and (B) TGA curve of $(NH_4)_{0.5}V_2O_5 \cdot mH_2O$ product.

dx.doi.org/10.1021/ic2005858 |*Inorg. Chem.* 2011, 50, 7421–7428

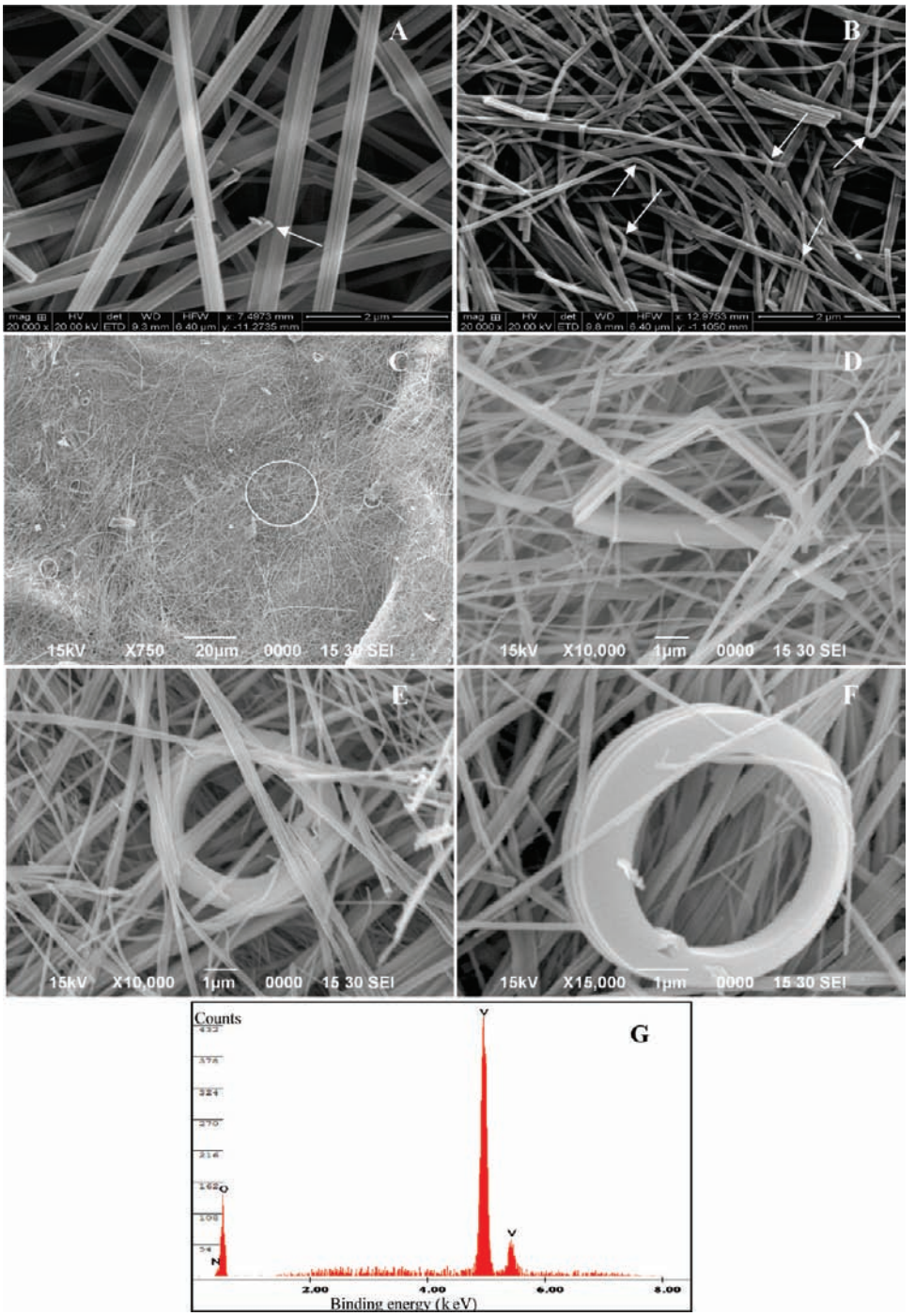

Figure 3. SEM images of the $(NH_4)_{0.5}V_2O_5 \cdot mH_2O$ products prepared at 160 °C for different reaction times: (A) 24, (B) 36, and (C−F) 48 h. (G) EDX spectrum of $(NH_4)_{0.5}V_2O_5 \cdot mH_2O$.

(965 and 996 cm^{-1}) as compared to standard V_2O_5 (~1020 cm^{-1}) arises from the formation of two inequivalent V═O groups.[16] The bands at 965 and 996 cm^{-1} are respectively assigned to the V═O stretching of distorted octahedral and distorted square pyramids. The bands at 841 and 539 cm^{-1} correspond to V−O−V bending and edge-sharing V−O stretching vibrations, respectively.[37] The band at 736 cm^{-1} could be assigned to a $V-OH_2$ stretching mode due to coordinated water.[38] The two bands at 3495 and 1628 cm^{-1} are attributed to the stretching and bending vibrations of water molecules, respectively.[39] The bands at 3180 and 1400 cm^{-1} are respectively assigned to the asymmetric stretching and the symmetric bending vibrations of NH_4^+, which indicated that ammonium ions could be present inside the interlayer space of the V_2O_5.[40]

Thermogravimetric analysis was carried out in order to determine the water content in the sample. The TGA curve shown in Figure 2B indicates the existence of two dehydration steps due to the removal of physical and chemically adsorbed water molecules. The first weight loss (14.5%) up to 230 °C can be attributed to the release of water adsorbed on the sample. The

dx.doi.org/10.1021/ic2005858 |*Inorg. Chem.* 2011, 50, 7421–7428

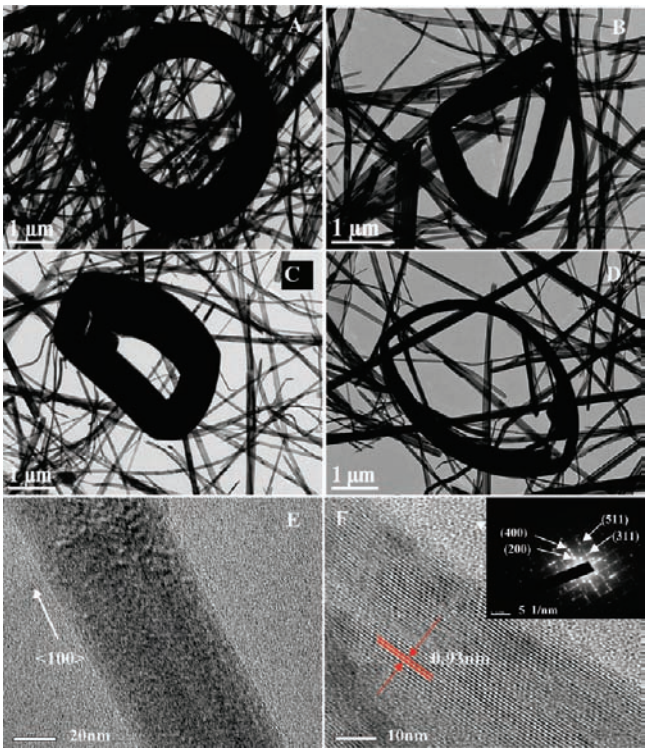

Figure 4. Representative TEM images of morphological evolution of (A) ring, (B) triangle, (C) rectangle, (D) oval, and (E) beltlike structures of $(NH_4)_{0.5}V_2O_5 \cdot mH_2O$ and (F) HRTEM image and SAED pattern (inset) of an individual $(NH_4)_{0.5}V_2O_5 \cdot mH_2O$ nanobelt.

second weight loss (9.4%) between 260 and 350 °C was ascribed to the departure of coordinated water molecules embedded between the V_2O_5 layers. The departure of ammonium ions was not observed presumably because most of the weight loss was due to water molecules.

The morphology of the products was examined by scanning electron microscopy. Parts A−F of Figure 3 show SEM images of $(NH_4)_{0.5}V_2O_5 \cdot mH_2O$ powders synthesized at 160 °C for different reaction times. After 24 h (Figure 3A) the product exhibits large-scale beltlike morphology with rectangular ends as shown by arrowheads. The width and thickness of the nanobelts are in the ranges of 402−551 and 235−305 nm, respectively, with typical lengths up to tens of micrometers. After 36 h (Figure 3B) the reaction product exhibits "bent-belt" morphology. This bending arises from the formation of a twin boundary at the (100) planes, which cause an abrupt 60° change in direction of the belt. After 48 h (Figure 3C−F), it is found that the resulting brown spongylike product exhibits large-scale beltlike morphology together with other geometrical shapes of $(NH_4)_{0.5}V_2O_5 \cdot mH_2O$ such as triangles, rings, and rectangles. The high-magnification SEM image (Figure 3D) reveals a triangular-like morphology with unequal sides. High-magnification SEM images (Figure 3E) show that the ringlike microstructures are made of packed nanobelts having a perfect circular shape and flat surfaces. Energy dispersive X-ray spectroscopy was also measured to determine the chemical composition of $(NH_4)_{0.5}V_2O_5 \cdot mH_2O$. The result from EDX shows (Figure 3G) that the product contains only V, N, and O (H cannot be detected by EDX).

The ring/triangle/oval and beltlike structures of the product were further checked using TEM and HRTEM. Parts A−E of Figure 4 show the TEM images of typical $(NH_4)_{0.5}V_2O_5 \cdot mH_2O$ rings/triangles/ovals and belts. A typical TEM image of a ring (Figure 4A) confirms that the thickness and width of the rings are found to be respectively ∼454 nm and ∼1 μm and their surface is smooth. Figure 4B shows the triangle shape with three unequal sides having a thickness of ∼143 nm and a width of ∼1 μm. The HRTEM image (Figure 4F) recorded from a single nanobelt shows that the interplanar spacing is about 0.93 nm, close to the separation between the adjacent two (001) lattice planes of monoclinic $(NH_4)_{0.5}V_2O_5 \cdot mH_2O$, as evidenced from the strong (001) peak of the PXRD pattern. This suggests that the $(NH_4)_{0.5}V_2O_5 \cdot mH_2O$ nanobelts exhibit a preferred growth direction along the (100) crystal axis. The selected area electron diffraction pattern taken from a single nanobelt (Figure 4F) and recorded from the (100) zone axis indicates that the nanobelts are single crystalline in nature.

We investigated the effect of calcination on the crystallization and morphology of the $(NH_4)_{0.5}V_2O_5 \cdot mH_2O$ belts/rings/triangles and ovals. After calcination at 350 °C for 2 h, $(NH_4)_{0.5}V_2O_5 \cdot mH_2O$ leads to pure crystalline V_2O_5. Parts A−D of Figure 5 show representative SEM images of post-calcined V_2O_5 sample, indicating that the individual morphologies of the precalcined $(NH_4)_{0.5}V_2O_5 \cdot mH_2O$ do not change after calcination. All of the PXRD peaks shown in Figure 5E could be attributed to the orthorhombic shcherbianite V_2O_5 phase (JCPDS card no. 86-2248), indicating that all intercalated molecules were driven out leading to V_2O_5. The energy dispersive X-ray spectrum analysis (Figure 5F) of V_2O_5 confirms that the product contains only V and O elements.

We also investigated the morphological evolution as a function of the amount of citric acid. A vanadium dioxide, VO_2, was obtained for a citric acid concentration of 0.02 M. The composition and purity of as-synthesized VO_2 was confirmed by X-ray diffraction. As shown in Figure 6A, the diffraction peaks of the resulting product correspond to the monoclinic crystalline phase of VO_2 ($P2/m$, JCPDS card no. 01-071-0290). Parts B and C of Figure 6 represent typical SEM images of VO_2 square nanoplates synthesized at 160 °C for 48 h. Square VO_2 nanoplatelets of ∼100 nm thick and ∼2 μm wide are obtained.

In this approach, NH_4VO_3 was used as the precursor with a hydrogen peroxide solution and citric acid. The basic reactions involved in the synthesis of $(NH_4)_{0.5}V_2O_5 \cdot mH_2O$ and V_2O_5 can be expressed as follows:

$$NH_4VO_3 + 4H_2O_2 \rightarrow NH_4[VO(O_2)_2] + 4H_2O + O_2 \quad (1)$$

$$NH_4[VO(O_2)_2] + H^+ \rightarrow H[VO(O_2)_2] + NH_4^+ \quad (2)$$

$$10H[VO(O_2)_2] \rightarrow [H_2V_{10}O_{28}]^{4-} + 4H_2O + 9O_2 \quad (3)$$

$$[H_2V_{10}O_{28}]^{4-} + 4NH_4^+ \rightarrow (NH_4)_{0.5}V_2O_5 \cdot mH_2O + {}^7/_2NH_4^+ \quad (4)$$

$$(NH_4)_{0.5}V_2O_5 \cdot mH_2O \xrightarrow{350\,°C/(2\,h)} V_2O_5 + mH_2O + {}^1/_2NH_3 \quad (5)$$

In the formation process, it is believed that hydrogen peroxide has a tendency to coordinate V^{5+} to form peroxo complexes.[41] Therefore, the dissolution of ammonium metavanadate in hydrogen peroxide leads to the formation of a yellow solution of diperoxo anions $[VO(O_2)_2]^-$ as observed in eq 1. Adding citric

dx.doi.org/10.1021/ic2005858 |Inorg. Chem. 2011, 50, 7421–7428

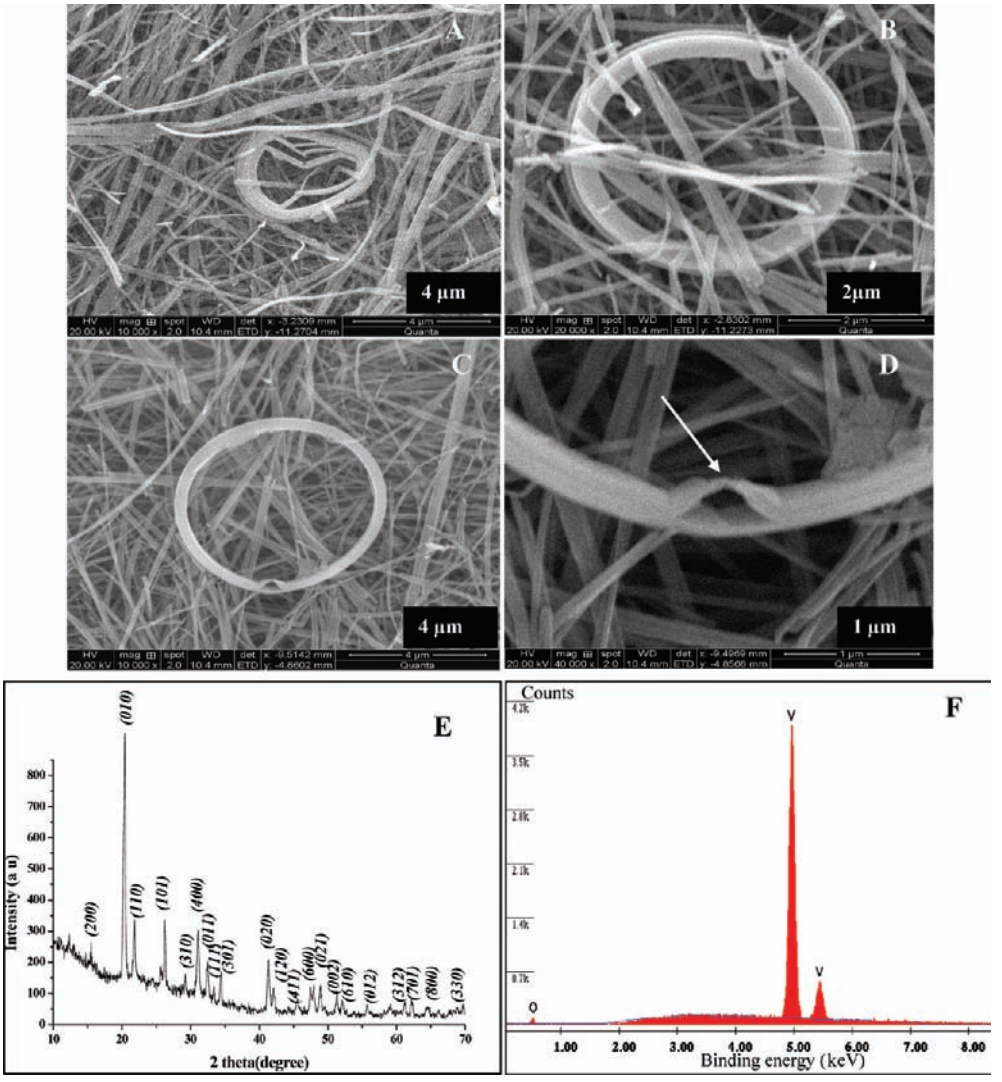

Figure 5. (A−D) SEM images of V_2O_5 product obtained after calcination of $(NH_4)_{0.5}V_2O_5 \cdot mH_2O$ at 350 °C for 2 h. (E) PXRD pattern and (F) EDX spectrum of the calcined V_2O_5 product.

acid gives a red solution (pH ≈ 2) of diperoxovanadic acid $H[VO(O_2)_2]$ as shown in eq 2. This diperoxovanadic acid appears to be unstable. It decomposes slowly with the evolution of oxygen gas, leading to the formation of an aqueous solution of decavanadic acid $[H_2V_{10}O_{28}]^{4-}$ as observed in eq 3. Then, the aqueous solution of decavanadic acid was subjected to hydrothermal treatment. At the initial stage of the hydrothermal process, decavanadic acid underwent condensation leading to the formation of a layered structure of $V_2O_5 \cdot mH_2O$ belts via a homogeneous nucleation and solution growth process. The presence of cations during the formation of the $V_2O_5 \cdot mH_2O$ leads to their intercalation within the vanadium oxide layers made of edge and corner sharing VO_5 square pyramids. The interlayer space in this layered V_2O_5 is occupied by water molecules and ammonium ions resulting in the formation of $(NH_4)_{0.5}V_2O_5 \cdot mH_2O$ belts. Wadsley[42] reported that the addition of cations does not significantly alter the structure and size of the V_2O_5 framework. Therefore, $(NH_4)_{0.5}V_2O_5 \cdot mH_2O$ should remain isostructural with the pristine $V_2O_5 \cdot xH_2O$ xerogel. The structure of $(NH_4)_{0.5}V_2O_5 \cdot mH_2O$ can be described as an assembly of stacked V_2O_5 bilayers. Vanadium coordination is based on $[VO_5]$ square pyramids with a short V═O double bond along the "*z*" axis perpendicular to the basal planes. Ammonium ions and water molecules are intercalated between the vanadium oxide layers.

The growth of ring, triangle, rectangle, and oval structures can be understood on the basis of this layered structure (Figure 7). Many models have been pushed forward to explain the formation of inorganic ringlike nanostructures. According to Liu and Zeng,[43] CdS rings were synthesized via the self-assembly of nanoparticles with an intrinsic hexagonal symmetry. Murray et al.[44] proposed an oriented attachment mechanism of nanoparticles to explain the formation of PbSe nanorings. A cation induced coiling growth mechanism was suggested by Liu and Xue[45] to describe the formation of vanadium pentoxide nanorings and microloops. Wang et al.[46] proposed the loop-by-loop coaxial, uniradius, self-coiling of a single nanobelt in order to explain the formation of ZnO nanorings in the vapor phase. A similar process was suggested by Shen et al.,[47] for the synthesis of $Ag_2V_4O_{11}$ nanorings and microloops from solutions.

These growth mechanisms cannot be extended to explain the formation of our $(NH_4)_{0.5}V_2O_5 \cdot mH_2O$ ringlike structures,

dx.doi.org/10.1021/ic2005858 |*Inorg. Chem.* 2011, 50, 7421–7428

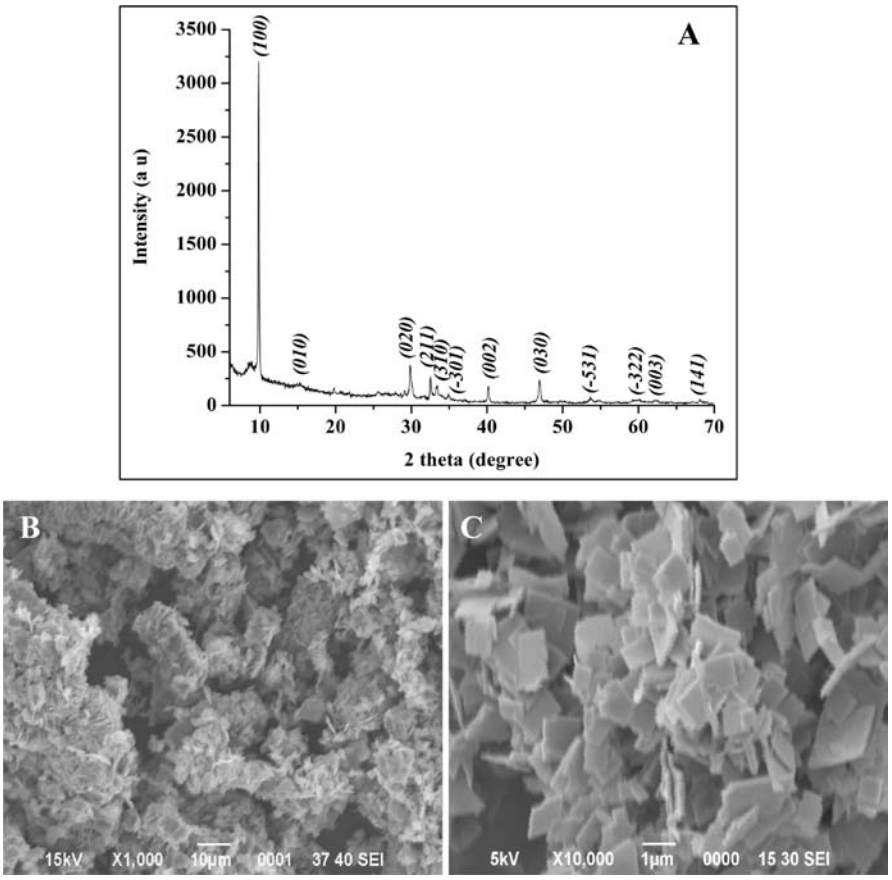

Figure 6. (A) PXRD pattern of as-prepared VO_2 product. Representative SEM images: (B) low magnification and (C) high magnification of the as-prepared VO_2 product.

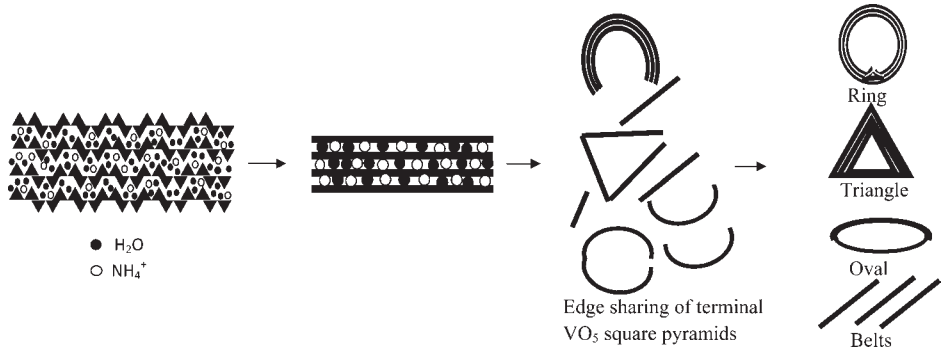

Figure 7. Schematic illustration of a possible process for the formation of $(NH_4)_{0.5}V_2O_5 \cdot mH_2O$ rings, triangles, ovals, and belts.

synthesized from solutions. Their morphologies are different from those of ZnO, CdS, V_2O_5, and $Ag_2V_4O_{11}$ nanorings. However, the "cation induced coiling growth mechanism", proposed by Liu et al., could, to a certain extent, be applied to the formation of $(NH_4)_{0.5}V_2O_5 \cdot mH_2O$ rings. This compound has a layered structure made of edge and corner sharing VO_5 square pyramids. These vanadium oxide sheets exhibit a polar structure arising from the $V{=}O^{\delta-}$ double bonds perpendicular to the layer plane within the VO_5 square pyramids. Moreover, NH_4^+ ions and water molecules intercalated between the vanadium oxide bilayers favor the flexibility of $(NH_4)_{0.5}V_2O_5 \cdot mH_2O$ nanobelts.[7b]

Positively charged NH_4^+ ions can be attracted by the $V{=}O^{\delta-}$ dipoles on both sides of the bilayers. According to the so-called "cation-induced coiling" model,[48] we may assume that, during the growth process of $(NH_4)_{0.5}V_2O_5 \cdot mH_2O$ nanobelts, asymmetric strain emerges as soon as the amount of adsorbed NH_4^+ becomes different on both the top or the bottom surface. When this asymmetric induced strain energy becomes larger than the elasticity energy, nanobelts will tend to bend or curve without fracture. Furthermore, we could expect that NH_4^+ ions intercalated at both ends of the belts can be easily removed as ammonia gas allowing the edges of vanadium oxide sheets to roll up. Edge sharing polar VO_5 square pyramids at both ends

dx.doi.org/10.1021/ic2005858 |*Inorg. Chem.* 2011, 50, 7421–7428

(Figure S2D of the Supporting Information) of the belt then connect (Figure S2A, B) in order to minimize the total energy arising from the electrostatic polarization energy and elastic deformation energy, leading to the formation of a perfect circular ring with a triangular tip (shown by arrowhead in Figure 5D). The curving/self-coiling of VO_5 pyramid sheets does not occur when the amount of NH_4^+ ions adsorbed on both, top and bottom, sides of $(NH_4)_{0.5}V_2O_5 \cdot mH_2O$ belts is the same. The reaction product also exhibits a triangular-like morphology. This special kind of morphology arises from the presence of twin boundaries within the (100) plane of a single belt. An abrupt 60° change in the direction of the belt then occurs, leading to the formation of triangles at both ends of the belt. This model might be too simple, and detailed formation mechanism of $(NH_4)_{0.5}V_2O_5 \cdot mH_2O$ triangles, rectangles, and ovals might require further investigation.

4. CONCLUSIONS

In summary, a novel and simple hydrothermal method has been successfully developed to prepare $(NH_4)_{0.5}V_2O_5 \cdot mH_2O$ xerogels with unusual morphologies: rings, triangles, rectangles, and ovals. On the basis of the layered structure of vanadium pentoxide, we report that these as-prepared $(NH_4)_{0.5}V_2O_5 \cdot mH_2O$ nanostructures are formed when two ends of a belt connect through edge and corner sharing of VO_5 square pyramids. A possible reaction mechanism and the growth processes involved in the formation of triangular/oval/belt and ringlike microstructures are discussed. Upon calcination, $(NH_4)_{0.5}V_2O_5 \cdot mH_2O$ xerogels, lead to the corresponding belts, rings, triangles, and ovals of the orthorhombic V_2O_5 shcherbianite phase. We are presently working on the enhancement of the yield of these fascinating $(NH_4)_{0.5}V_2O_5 \cdot mH_2O$ rings/triangles and ovals by varying the experimental conditions, such as the reaction temperature, pH, and addition of surfactants, etc. Better yields would give enough products to study their chemical and physical properties.

■ ASSOCIATED CONTENT

Supporting Information. Figures showing representative SEM and TEM images of the resulting product. This material is available free of charge via the Internet at http://pubs.acs.org.

■ AUTHOR INFORMATION

Corresponding Author

*E-mail: gtchandrappa@yahoo.co.in. Phone: +91 80 22961350. Fax: +91 80 22100187.

■ ACKNOWLEDGMENT

G.T.C. gratefully acknowledges the Department of Science and Technology, New Delhi, India, for financial support and Prof. S. Ranganatha, Department of Mechanical Engineering, UVCE, Bangalore for the SEM measurements. P.C. is thankful to Bangalore University for awarding a fellowship to carry out this work.

■ REFERENCES

(1) (a) Wang, Y.; Wu, K. *J. Am. Chem. Soc.* **2005**, *127*, 9686. (b) Sun, Y.; Xia, Y. *Science* **2002**, *298*, 2176. (c) Rao, C. N. R.; Nath, M. *Dalton Trans.* **2003**, *1*, 1. (d) Yin, Y.; Rioux, R. M.; Erdonmez, C. K.; Hughes, S.; Somorja, G. A.; Alivisatos, A. P. *Science* **2004**, *304*, 711. (e) Chen, J.; Saeki, F.; Wiley, B. J.; Cang, H.; Cobb, M. J.; Li, Z. Y.; Au, L.; Zhang, H.; Kimmey, M. B.; Li, X.; Xia, Y. *Nano Lett.* **2005**, *5*, 473. (f) Caruso, F.; Caruso, R. A.; Mohwald, H. *Science* **1998**, *282*, 1111. (g) Wu, G. S.; Zhang, L. D.; Cheng, B. C.; Xie, T.; Yuan, X. Y. *J. Am. Chem. Soc.* **2004**, *126*, 5976. (h) Rao, C. N. R.; Deepak, F. L.; Gundiah, G.; Govindaraj, A. *Prog. Solid State Chem.* **2003**, *31*, 5. (i) Xia, Y. N.; Yang, P. D.; Sun, Y. G.; Wu, Y. Y.; Mayers, B.; Gates, B.; Yin, Y. D.; Kim, F.; Yan, H. Q. *Adv. Mater.* **2003**, *15*, 353.

(2) (a) Takahashi, K.; Limmer, S. J.; Wang, Y.; Cao, G. *J. Phys. Chem. B* **2004**, *108*, 9795. (b) Poizot, P.; Grugeon, S.; Dupont, L.; Tarascon, J. M. *Nature* **2000**, *407*, 496.

(3) (a) Karunakaran, C.; Senthilvelan, S. J. *Colloid Interface Sci.* **2005**, *289*, 466. (b) Livage, J. *Chem. Mater.* **1991**, *3*, 578.

(4) (a) Talledo, A.; Granqvist, C. G. *J. Appl. Phys.* **1995**, *77*, 4655. (b) Liu, P.; Lee, S. H.; Tracy, C. E.; Tuener, J. A.; Pitts, J. R.; Deb, S. K. *Solid State Ionics* **2003**, *165*, 223. (c) Takahashi, K.; Wang, Y.; Cao, G. Z. *Appl. Phys. Lett.* **2005**, *86*, 053102.

(5) (a) Gu, G.; Schmid, M.; Chiu, P. W.; Minett, A.; Fraysse, J.; Kim, G. T.; Roth, S.; Kozlov, M.; Munoz, E.; Baughman, R. H. *Nat. Mater.* **2003**, *2*, 316. (b) Biette, L.; Carn, F.; Maugey, M.; Achard, M. F.; Maquet, J.; Steunou, N.; Livage, J.; Serier, H.; Backov, R. *Adv. Mater.* **2005**, *17*, 2970.

(6) (a) Liu, J. F.; Wang, X.; Peng, Q.; Li, Y. D. *Adv. Mater.* **2005**, *17*, 764. (b) Serier, H.; Achard, M. F.; Babot, O.; Steunou, N.; Maquet, J.; Livage, J.; Leroy, C.; Backov, R. *Adv. Funct. Mater.* **2006**, *16*, 1745. (c) Leroy, C. M.; Achard, M. F.; Babot, O.; Steunou, N.; Masse, P.; Livage, J.; Binet, L.; Brun, N.; Backov, R. *Chem. Mater.* **2007**, *19*, 3988.

(7) (a) Durupthy, O.; Steunou, N.; Coradin, T.; Livage, J. *J. Phys. Chem. Solids* **2006**, *67*, 944. (b) Wu, X. C.; Tao, Y. R.; Dong, L.; Hong, J. M. *J. Mater. Chem.* **2004**, *14*, 901.

(8) Krumeich, F.; Muhr, H. J.; Niederberger, M.; Bieri, F.; Schnyder, B.; Nesper, R. *J. Am. Chem. Soc.* **1999**, *121*, 8324.

(9) Luca, V.; Maclachlan, D. J.; Hook, J. M.; Withers, R. *Chem. Mater.* **1995**, *7*, 2220.

(10) Luca, V.; Hook, J. M. *Chem. Mater.* **1997**, *9*, 2731.

(11) Chandrappa, G. T.; Steunou, N.; Livage, J. *Nature* **2002**, *416*, 702.

(12) (a) Zhou, F.; Zhao, X.; Yuan, C.; Li, L. *Cryst. Growth Des.* **2008**, *8*, 723. (b) W., A., Jr.; Ribeiro, C.; Leite, E. R.; Mastelaro, V. R. *Cryst. Growth Des.* **2009**, *9*, 3626.

(13) Li, Y. D.; Liao, H. W.; Ding, Y.; Fan, Y.; Zhang, Y.; Qian, Y. T. *Inorg. Chem.* **1999**, *38*, 1382.

(14) (a) Rothschild, A.; Sloan, J.; Tenne, R. *J. Am. Chem. Soc.* **2000**, *122*, 5169. (b) Durupthy, O.; Steunou, N.; Coradin, T.; Maquet, J.; Bonhomme, C.; Livage, J. *J. Mater. Chem.* **2005**, *15*, 1090.

(15) Wang, Y.; Cao, G. *Chem. Mater.* **2006**, *18*, 2787.

(16) Pinna, N.; Wild, U.; Urban, J.; Schlogl, R. *Adv. Mater.* **2003**, *15*, 329.

(17) Han, W.; Fan, S.; Li, Q.; Hu, Y. *Science* **1997**, *277*, 1287.

(18) Wang, X.; Xi, G.; Xiong, S.; Liu, Y.; Xi, B.; Yu, W.; Qian, Y. *Cryst. Growth Des.* **2007**, *7*, 930.

(19) Yang, R. S.; Wang, Z. L. *J. Am. Chem. Soc.* **2006**, *128*, 1466.

(20) Wang, Y.; Zang, K.; Chua, S.; Sander, M. S.; Tripathy, S.; Fonstad, C. G. *J. Phys. Chem. B* **2006**, *110*, 11081.

(21) Zhu, F.; Yang, Z. X.; Zhou, W. M.; Zhang, Y. F. *Phys. Status Solidi A* **2006**, *203*, 2024.

(22) Shen, G. Z.; Bando, Y.; Zhi, C. Y.; Yuan, X. L.; Sekiguchi, T.; Golberg, D. *Appl. Phys. Lett.* **2006**, *88*, 243106.

(23) Cho, K. S.; Talapin, D. V.; Gaschler, W.; Murray, C. B. *J. Am. Chem. Soc.* **2005**, *127*, 7140.

(24) Hao, X.; Wu, Y.; Zhan, J.; Yang, J.; Xu, X.; Jiang, M. *J. Phys. Chem. B* **2005**, *109*, 19188.

(25) Duan, J.; Yang, S.; Liu, H.; Gong, J.; Huang, H. B.; Zhao, X. N.; Tang, J.; Zhang, R.; Du, Y. W. *J. Cryst. Growth* **2005**, *283*, 291.

(26) Gao, P. X.; Ding, Y.; Mai, W. J.; Hughes, W. L.; Lao, C.; Wang, Z. L. *Science* **2005**, *309*, 1700.

(27) Kong, X. Y.; Ding, Y.; Yang, R. S.; Wang, Z. L. *Science* **2004**, *303*, 1348.
(28) Yang, R. S.; Ding, Y.; Wang, Z. L. *Nano Lett.* **2004**, *4*, 1309.
(29) Kong, X. Y.; Wang, Z. L. *Nano Lett.* **2003**, *3*, 1625.
(30) Yan, F.; Goedel, W. A. *Nano Lett.* **2004**, *4*, 1193.
(31) Wang, J. X.; Xie, S. S.; Yuan, H. J.; Yan, X. Q.; Liu, D. F.; Gao, Y.; Zhou, Z. P.; Song, L.; Liu, L. F.; Zhao, X. W.; Dou, X. Y.; Zhou, W. Y.; Wang, G. *Solid State Commum.* **2004**, *131*, 435.
(32) Zhang, H. F.; Wang, C. M.; Buck, E. C.; Wang, L. S. *Nano Lett.* **2003**, *3*, 577.
(33) Zhang, H. F.; Wang, C. M.; Wang, L. S. *Nano Lett.* **2002**, *2*, 941.
(34) Amelinckx, S.; Zhang, X. B.; Bernaerts, D.; Zhang, X. F.; Ivanov, V.; Nagy, J. B. *Science* **1994**, *265*, 635.
(35) Trikalitis, P. N.; Petkov, V.; Kanatzidis, M. G. *Chem. Mater.* **2003**, *15*, 3337.
(36) Liu, Y. J.; Cowen, J. A.; Kaplan, T. A.; Degroot, D. C.; Schindler, J.; Kannewurf, C. R.; Kanatzidis, M. G. *Chem. Mater.* **1995**, *7*, 1616.
(37) Liu, X.; Huang, C.; Qiu, J.; Wang, Y. *Appl. Surf. Sci.* **2006**, *253*, 2747.
(38) Azambre, B.; Hudson, M. J.; Heintz, O. *J. Mater. Chem.* **2003**, *13*, 385.
(39) Vanova, T.; Harizanova, A. *Mater. Res. Bull.* **2005**, *40*, 411.
(40) Dobley, A.; Ngala, K.; Yang, S. F.; Zavalij, P. Y.; Whittingham, M. S. *Chem. Mater.* **2001**, *13*, 4382.
(41) Butler, A.; Clague, M. J.; Meister, G. E. *Chem. Rev.* **1994**, *94*, 625.
(42) Wadsley, A. D. *Acta Crystallogr.* **1955**, *8*, 695.
(43) Liu, B.; Zeng, H. C. *J. Am. Chem. Soc.* **2005**, *127*, 18262.
(44) Cho, K. S.; Talapin, D. V.; Gaschler, W.; Murray, C. B. *J. Am. Chem. Soc.* **2005**, *127*, 7140.
(45) Liu, J.; Xue., D. *Nanoscale Res. Lett.* **2010**, *5*, 1619.
(46) Kong, X. Y.; Ding, Y.; Yang, R. S.; Wang, Z. L. *Science* **2004**, 303.
(47) Shen, G. Z.; Chen, D. *J. Am. Chem. Soc.* **2006**, *128*, 11762.
(48) Schmidt, O. G.; Eberl, K. *Nature* **2001**, *410*, 168.